Journal of The Electrochemical Society, **152** (5) A1001-A1010 (2005)
0013-4651/2005/152(5)/A1001/10/$7.00 © The Electrochemical Society, Inc.

Extraction of Layerwise Conductivities in Carbon-Enhanced, Multilayered $LiFePO_4$ Cathodes

C.-W. Wang,[a] A. M. Sastry,[a,b,*,z] K. A. Striebel,[c,*] and K. Zaghib[d,*]

[a]*Department of Mechanical Engineering,* [b]*Department of Biomedical Engineering, University of Michigan, Ann Arbor, Michigan 48109-2125, USA*
[c]*Lawrence Berkeley National Laboratory, Environmental Energy Technologies Division, Berkeley, California 94720, USA*
[d]*Institut de Recherche d'Hydro Quebec, Varennes PQ J3X 1S1, Canada*

We performed experimental studies to determine electronic properties of multilayered $LiFePO_4$ cathodes in order to quantify reductions in $LiFePO_4$ matrix resistivity and/or contact resistances between matrices and current collectors by addition of carbon black and graphite. In order to extract these layerwise and interlayer properties, we extended the Schumann-Gardner approach to analysis of a four-point probe experiment and solved the resulting coupled nonlinear equations numerically. We studied five cathodes with varying amounts (3-12 wt %) and types (carbon black, graphite) of conductive additives. $LiFePO_4$ particles within the electrodes were precoated with carbon before mixing with additives and binder. Experimental results showed reductions of ~62% in electrical resistivities of $LiFePO_4$ matrix with addition of carbon black from 3 to 10 wt %; addition of graphite additives produced only small reductions. For concentrations above 6 wt % of conductive additives, homogeneous electronic resistivities were observed. Contact resistances at interfaces between $LiFePO_4$ matrix and carbon coating of current collector and between carbon coating and current collector were similar in all cases, indicating consistency in manufacturing. Future work will focus on combining models for capacitive loss with models for conductive properties, along with experimental verifications.
 [DOI: 10.1149/1.1890766]

Manuscript submitted July 2, 2004; revised manuscript received October 15, 2004. Available electronically April 11, 2005.

The low-cost, low environmental impact, and high theoretical specific capacity of $LiFePO_4$-based composites have made them extremely attractive materials for positive electrodes in Li-ion cells. The bulk electronic conductivity of $LiFePO_4$, however, is reportedly quite low, ranging from 10^{-10} to 10^{-9} S cm^{-1};[1] this electronic/ionic resistance has been blamed for losses in its relatively high capacity (170 mAh/g) during high-rate discharge.[2-4]

The constituents of the $LiFePO_4$ electrode include $LiFePO_4$ particles, conductive additives, binder, and the metallic current collector. Commonly, electrodes comprise at least two layers (*i.e.*, composite active material and current collector). Increasingly, though, current collectors are being surface-treated to reduce interfacial resistance between metallic current collectors and active material layers;[5,6] this effectively increases the total number of layers within the current collector in terms of analysis of the contribution to conductivity of each layer. In order to understand the role of each constituent and to further optimize electrode overall performance, a technique to extract individual layer's conductivity is needed. Here we extend our prior technique[7] for analysis of conductivity of multiphase layers containing conductive additives to extract layerwise conductivities and interfacial resistances. With this technique, we ultimately aim to optimize electrode performance via proper design of conductive additives and surface treatments.

To date, three basic approaches have been used to improve the high-rate performance of $LiFePO_4$, including (*i*) doping of $LiFePO_4$ with conductive metals;[1,8] (*ii*) use of carbon additives to a $LiFePO_4$ matrix;[2,9] and (*iii*) surface coating of $LiFePO_4$ particles with thin layers of carbon.[4,10] Doping has produced improvements in conductivity, of bulk $LiFePO_4$, of 10^{-2} S cm^{-1} with doping 1.0 atom % Nb *vs.* 10^{-10}-10^{-9} S cm^{-1}[1] without dopant; moreover, addition of metallic particles (*e.g.*, Nb, of density 8.6 g/cm^3[11]) drives up the overall electrode mass of these systems more than addition of carbon (2.25 g/cm^3, per Ref. 11).

Chen and Dahn[12] have pointed out that volumetric energy density and gravimetric energy density drop from 2.05 to 1.6 Wh/cm^3, and from 0.57 to 0.48 Wh/g, respectively, with addition of 15 wt % carbon additive. Thus, the addition of lower density carbons merits investigation to identify the best ratios of geometries and densities of conductive particles, because they both affect percolation onset. Though solutions for percolation have recently been reported in a wide range of systems, including 2D and 3D systems of ellipses and ellipsoids,[13,14] generalized solutions for polydisperse systems are available for only certain special cases.[15,16] Empirically,[10] it has been shown that the use of the second approach, *i.e.*, addition of carbon black mixed with $LiFePO_4$ particles, provides cathode powders of sufficient electronic conductivity for carbon additives of 2-30 wt %.[3,9,12,17] However, the process of adding carbon black of sufficiently uniform distribution in the matrix is costly, because it is both time- and energy-consuming.[10] Further, addition of binder can produce additional segregation, which must be monitored.[10]

Thus, the third approach of adding carbon coatings to $LiFePO_4$ particles presently appears attractive.[12] Chen and Dahn[12] produced an $LiFePO_4$/C composite by addition of sugar to $LiFePO_4$ particles before heating, resulting in a 3.5 wt % carbon coating of particles. This composite showed comparable rate performance to 15 wt % carbon additives reported by Huang *et al.*[3] Improvements in both matrix conductivity and in functional performance of composite cathodes have both been demonstrated by this general approach. Improvement in electronic conductivity in composite cathodes has been demonstrated via addition of 30 wt % carbon-included, spray-pyrolyzed, pelletized $LiFePO_4$, from an original conductivity of 10^{-10} S cm^{-1} to 0.1 S cm^{-1}.[10] Ravet and co-workers,[4] which compared the electroactivity of natural and synthetic $LiFePO_4$ ores, and demonstrated >82% of theoretical capacity (170 mAh g^{-1}), *vs.* below <80% for untreated ores, could be achieved by 1 wt % of carbon coating around both nature and synthetic $LiFePO_4$ ores. They further showed that the cycle ability of both nature and synthetic $LiFePO_4$ ores improved with carbon coating. Huang and co-workers similarly demonstrated ~90% theoretical capacity in composite cathodes containing a 15 wt % carbon coating of $LiFePO_4$ particles, at C/2 with good stability.[3]

Conversely, Chung and co-workers[1] observed that at high firing temperature (>800°C) the fraction of the Fe_2P phase increases, as does the electronic conductivity of the undoped $LiFePO_4$. They postulated that the use of carbon coating to increased conductivity was a result of a solid-state doping effect. Regardless of mechanism, higher firing temperatures appear to be another possible avenue toward improvement of $LiFePO_4$ conductivity.

Though both four-point[1] and two-point[10] probe techniques have been used to measured electronic conductivity of $LiFePO_4$ in bulk or pellet form, no analytical solutions enabling extraction of layerwise resistivities (conductivities) and interfacial resistances from

* Electrochemical Society Active Member.
z E-mail: amsastry@umich.edu

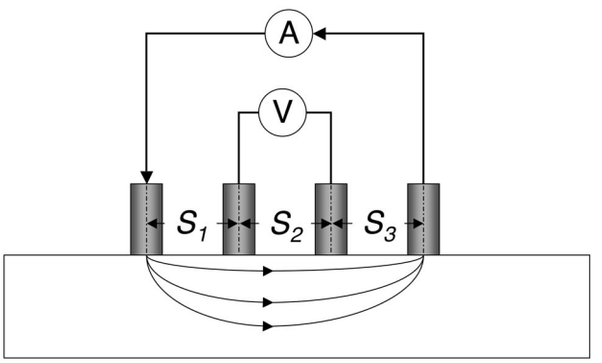

Figure 1. The four-point-probe setup.

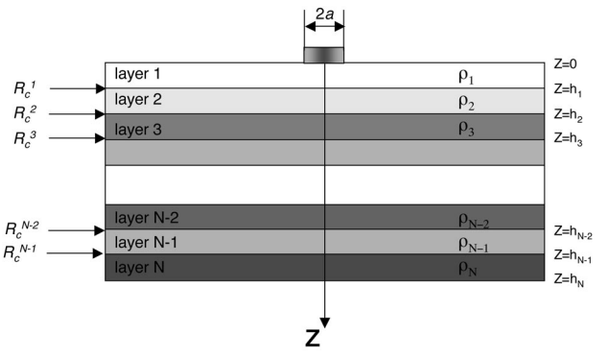

Figure 2. A schematic of an *N*-layered material for the theoretical model developed.

nondestructive surface measurements, to the authors' knowledge, have been published to date for multilayer laminates such as electrodes. Because both heat-treatment[8] and compression are commonly used to post-process cathodes, use of bulk conductivities, or conductivities of pelletized $LiFePO_4$, is questionable: electronic conductivity of $LiFePO_4$ matrix in real electrodes is required to identify optimal carbon loading types and densities.

Here, we extend the traditional four-point probe technique to allow extraction of electronic resistivity of each layer and interfacial resistance at each interface from measured voltages with different sets of probe spacing, extending our earlier work on the subject.[7,18] We used this approach to determine *in situ* electronic conductivity of $LiFePO_4$ matrices with varying amounts and types of carbon additives. Following the Schumann-Gardner[19,20] approach, the voltage measured at the surface of the electrode was derived as a function of probe spacing, input current, electrical properties, and thicknesses of the sublayers. Hence, the electrical properties of each sublayer could be extracted from an assumed voltage function.

Experimental

A solution for layer-wise resistivities, and interfacial resistance in a two-layer sheet, using data from an in-line, four-point probe technique[7] is first briefly outlined. Derivations of voltage functions for multilayered structures are then derived. The numerical approach used to extract the electrical properties (resistivity and contact resistance of each sublayer) from the measured sets of voltage and current, is also presented, followed by a section detailing our experimental approach.

Solutions for current and voltage distributions in the four-probe experiment.—The model inline four-point-probe setup[7,19,20] is illustrated in Fig. 1; a single probe delivering current I into an N-layered structure is shown in Fig. 2. Each layer is assumed to be homogeneous and isotropic with respect to resistivity, *i.e.*, measured resistivity is assumed constant and independent of direction of applied current within any layer. Further, no sources of current are assumed to be present within any layer. Collectively, these assumptions allow solution for voltage within any layer, *i.e.*, V_i for the ith layer, via Laplace's equation. In cylindrical coordinates, we have

$$\frac{\partial^2 V(r,z)_i}{\partial r^2} + \frac{1}{r}\frac{\partial V_i(r,z)}{\partial r} + \frac{\partial^2 V_i(r,z)}{\partial z^2} = 0 \qquad [1]$$

which can be solved by separation of variables.

Solutions of Eq. 1 are linear combinations of Bessel functions of the first and second kind; in the present case, we can express a solution in terms of Bessel functions of the first kind only, because the finite value of the voltage function requires that the coefficient of the Bessel function of the second kind be zero. Solutions for the second term are obtainable in terms of $e^{-\lambda z}$ and $e^{\lambda z}$. Solution of Laplace's equation for each layer can thus be expressed as

$$V_i(r,z) = \int_0^\infty A_i(\lambda)J_0(\lambda r)e^{-\lambda z}d\lambda + \int_0^\infty B_i(\lambda)J_0(\lambda r)e^{\lambda z}d\lambda \qquad [2]$$

where functions $A_i(\lambda)$ and $B_i(\lambda)$ can be obtained with application of appropriate boundary conditions. There are $2N$ boundary conditions required to find N sets of $A_i(\lambda)$ and $B_i(\lambda)$ for an N-layered electrode. These conditions are described in the following paragraphs, and involve, 1. total current input, 2. finite voltage step change, 3. constant current at the boundary, and 4. current flow from the probe.

1. The total current input from the cylindrical shape of probe with radius a at the probe-first layer interface ($z = 0$) is

$$j(r) = -\frac{1}{\rho_1}\frac{\partial V_1(r,z=0)}{\partial z} = \int_0^\infty \lambda\left[\frac{A_1(\lambda) - B_i(\lambda)}{\rho_1}\right]J_0(\lambda r)d\lambda \qquad [3]$$

If the function of current intensity $j(r)$ is known, the relationship between $A_1(\lambda)$ and $B_1(\lambda)$ can be obtained via Hankel transform pairs as

$$g(\lambda) = \int_0^\infty rf(r)J_0(\lambda r)dr$$

$$f(r) = \int_0^\infty \lambda g(\lambda)J_0(\lambda r)d\lambda \qquad [4]$$

Various assumptions concerning the current distribution through the probe input to the N-layered system have been made[19-22] as illustrated in Fig. 3; their effects on results have previously been compared extensively.[23] The mathematical forms of several key assumptions are given as follows, with I designating the total current input from the probe: Equipotential beneath the probe[19]

$$-\frac{1}{\rho_1}\frac{\partial V_1(r,z)}{\partial z} = \begin{cases} \dfrac{I}{2\pi a\sqrt{a^2 - r^2}} & \text{if } |r| \leqslant a \text{ and } z = 0 \\ 0 & \text{if } |r| > a \text{ and } z = 0 \end{cases} \qquad [5]$$

Uniform current distribution[21]

$$-\frac{1}{\rho_1}\frac{\partial V_1(r,z)}{\partial z} = \begin{cases} \dfrac{I}{\pi\alpha^2} & \text{if } |r| \leqslant a \text{ and } z = 0 \\ 0 & \text{if } |r| > a \text{ and } z = 0 \end{cases} \qquad [6]$$

Dirac delta current distribution[22]

$$-\frac{1}{\rho_1}\frac{\partial V_1(r,z)}{\partial z} = \frac{I}{2\pi r}\delta(r - a) \qquad [7]$$

In our work, we adopt the Schumann-Gardner[19,20] assumption of Eq. 7, though the differences among results from the three models are only $\sim$10%.[23,24] Our rationale is twofold. First, using this expres-

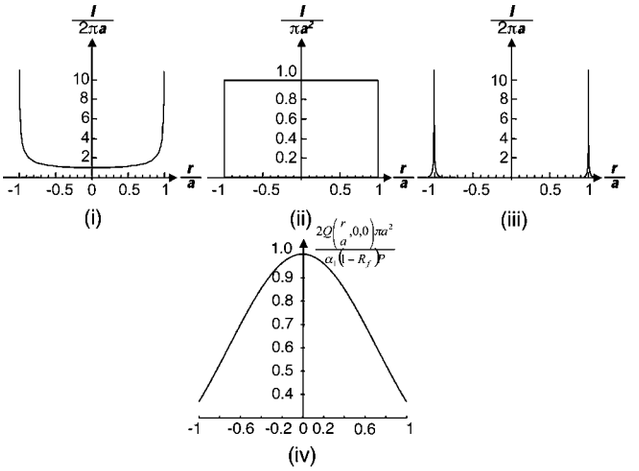

Figure 3. Three possible current distributions, including (i) equipotential under a probe, as in Eq. 6, (ii) uniform current intensity, as in Eq. 7, and (iii) Dirac delta as in Eq. 8, and (iv)A Gaussian-type heat source, used in Ref. 25.

sion enforces constant voltage under the probe. Second, the current is restricted to fall between the probe radii.

In related work, Li and Zhang[25] analyzed the temperature profile of multilayered anisotropic material heated via laser beam, an analog to the present study. In their paper, the heat source profile had a Gaussian spatial profile (with radius a), of

$$Q_1(r,z,t) = \frac{1}{2}\frac{\alpha_1(1-R_f)P}{\pi a^2}\exp\left(-\frac{r^2}{a^2} - \alpha_1 z + j\omega t\right) + \delta O \quad [8]$$

where α_1 denotes the optical absorption coefficient of the first layer and R_f is the reflectivity at the surface of the first layer. The normalized laser heat source profile at the surface of anisotropic material at time $t = 0$ is shown by Fig. 3 (iv), which has a maximum intensity at the center of the profile due to fast dissipation of heat at the outer radii. The Dirac delta is a good model for current profile for a perfect conductor as in Fig. 3 (iii), due to no potential difference within probe radii. For a good conductor, Eq. 5 is a reasonable model because of small potential difference within the probe.

If Eq. 5 is adopted to describe current intensity, the relationship between $A_1(\lambda)$ and $B_1(\lambda)$ at Eq. 3 can be calculated using a Hankel transform via Eq. 4, as

$$A_1(\lambda) - B_1(\lambda) = \rho_1\int_0^\infty rj(r)J_0(r)dr = \frac{I\rho_1\sin(a\lambda)}{2\pi a\lambda} \quad [9]$$

It is then advantageous for simplification of subsequent calculations to redefine functions $A_i(\lambda)$ and $B_i(\lambda)$ from Eq. 2 in terms of $\theta_i(\lambda)$ and $\psi_i(\lambda)$ for simplification as

$$A_1(\lambda) - B_1(\lambda) = [\theta_1(\lambda) - \psi_1(\lambda)]\frac{I\rho_1\sin(a\lambda)}{2\pi a\lambda} \quad [10]$$

where

$$\theta_1(\lambda) - \psi_1(\lambda) = 1 \quad [11]$$

Similarly, we can write the voltage function of each sublayer at Eq. 4 in terms $\theta_i(\lambda)$ and $\psi_i(\lambda)$ as

$$V_i(r,z) = \int_0^\infty A_i(\lambda)J_0(\lambda r)e^{-\lambda z}d\lambda + \int_0^\infty B_i(\lambda)J_0(\lambda r)e^{\lambda z}d\lambda$$
$$= \frac{I\rho_1}{2\pi a}\left[\int_0^\infty \frac{\theta_i(\lambda)}{\lambda}\sin(\lambda a)J_0(\lambda r)e^{-\lambda z}d\lambda + \int_0^\infty \frac{\psi_i(\lambda)}{\lambda}\sin(\lambda a)J_0(\lambda r)e^{\lambda z}d\lambda\right] \quad [12]$$

2. At the interface $z = h_i$, there is a finite voltage step at the interface between two adjacent layers, which is determined by electrical contact resistance R_c^i. Then the boundary conditions at the intermediate layers, such as the interface of the ith and the $(i + 1)$-th adjacent layers satisfy

$$V_i(r,z)|_{z=h_i} - V_{i+1}(r,z)|_{z=h_2} = R_c^i\left(-\frac{1}{\rho_i}\frac{\partial V_i(r,z)}{\partial z}\bigg|_{z=h_i}\right) \times (i = 1,2,3,\ldots N-1) \quad [13]$$

3. At the interface, $z = h_i$, the current density is the same across the boundary as

$$-\frac{1}{\rho_i}\frac{\partial V_i(r,z)}{\partial z}\bigg|_{z=h_i} = -\frac{1}{\rho_{i+1}}\frac{\partial V_{i+1}(r,z)}{\partial z}\bigg|_{z=h_i} \times (i = 1,2,3,\ldots N-1) \quad [14]$$

4. No current flows from the electrode, $z = h_N$, *i.e.*, we assume the specimen is tested on an insulated boundary, per

$$j(r) = -\frac{1}{\rho_N}\frac{\partial V_N(r,z)}{\partial z}\bigg|_{z=h_N} = 0 \quad [15]$$

The details of derivation have been discussed previously.[7] The parameters $\theta_i(\lambda)$ and $\psi_i(\lambda)$ (as $i = 1,2,\ldots,N$) can be determined based on the boundary conditions Eq. 11 and 13-15. They can be expressed in terms of matrix form as

$$[1,-1]\begin{bmatrix}\theta_1(\lambda)\\ \psi_1(\lambda)\end{bmatrix} = 1 \quad [16]$$

$$[1,-e^{-2\lambda h_N}]\begin{bmatrix}\theta_N(\lambda)\\ \psi_N(\lambda)\end{bmatrix} = 0 \quad [17]$$

$$\begin{bmatrix}\theta_i(\lambda)\\ \psi_i(\lambda)\end{bmatrix} = \begin{bmatrix}\frac{(\lambda R_c^i + \rho_i + \rho_{i+1})}{2\rho_{i+1}}, & -\frac{e^{2\lambda h_i}(\lambda R_c^i + \rho_i - \rho_{i+1})}{2\rho_{i+1}}\\ \frac{e^{-2\lambda h_i}(\lambda R_c^i - \rho_i + \rho_{i+1})}{2\rho_{i+1}}, & \frac{(-\lambda R_c^i + \rho_i + \rho_{i+1})}{2\rho_{i+1}}\end{bmatrix} \times \begin{bmatrix}\theta_{i+1}(\lambda)\\ \psi_{i+1}(\lambda)\end{bmatrix} \quad [18]$$

If we defined a matrix $\mathbf{M}_i$ as

$$\mathbf{M}_1 = \begin{bmatrix}\frac{(\lambda R_c^i + \rho_i + \rho_{i+1})}{2\rho_{i+1}}, & -\frac{e^{2\lambda h_i}(\lambda R_c^i + \rho_i - \rho_{i+1})}{2\rho_{i+1}}\\ \frac{e^{-2\lambda h_i}(\lambda R_c^i - \rho_i + \rho_{i+1})}{2\rho_{i+1}}, & \frac{(-\lambda R_c^i + \rho_i + \rho_{i+1})}{2\rho_{i+1}}\end{bmatrix} \quad [19]$$

and plugging Eq. 18 recursively back into itself starting from (i = 1), we find, with combination of Eq. 17

$$\begin{bmatrix}\theta_1(\lambda)\\ \psi_1(\lambda)\end{bmatrix} = \mathbf{M}\begin{bmatrix}\theta_2(\lambda)\\ \psi_2(\lambda)\end{bmatrix} = \mathbf{M}_1\mathbf{M}_2\mathbf{M}_3\cdots\mathbf{M}_{N-1}\begin{bmatrix}\theta_N(\lambda)\\ \psi_N(\lambda)\end{bmatrix}$$

$$= \mathbf{M}_1\mathbf{M}_2\mathbf{M}_3\cdots\mathbf{M}_{N-1}\begin{bmatrix}1\\ e^{-2\lambda h_N}\end{bmatrix}\theta_N(\lambda)$$

$$\times[1,-1]\prod_{i=1}^{N-1}\mathbf{M}_i\begin{bmatrix}1\\ e^{-2\lambda h_N}\end{bmatrix}\theta_N(\lambda) = 1 \qquad [20]$$

With the relationship of Eq. 19, this equation can be reduced to

$$[1\ -1]\prod_{i=1}^{N-1}\mathbf{M}_i\begin{bmatrix}1\\ e^{-2\lambda h_N}\end{bmatrix}\theta_N(\lambda) = 1$$

and $\theta_N(\lambda)$ can be obtained, as

$$\theta_N(\lambda) = \frac{1}{[1,-1]\prod_{i=1}^{N-1}\mathbf{M}_i\begin{bmatrix}1\\ e^{-2\lambda h_N}\end{bmatrix}} \qquad [21]$$

Combining Eq. 21 with Eq. 19, we find that $\theta_1(\lambda)$ and $\psi_1(\lambda)$ can be expressed as

$$\theta_1(\lambda) = \frac{[1,0]\prod_{i=1}^{N-1}\mathbf{M}_i\begin{bmatrix}1\\ e^{-2\lambda h_N}\end{bmatrix}}{[1,-1]\prod_{i=1}^{N-1}\mathbf{M}_i\begin{bmatrix}1\\ e^{-2\lambda h_N}\end{bmatrix}}$$

$$\psi_1(\lambda) = \frac{[0,1]\prod_{i=1}^{N-1}\mathbf{M}_i\begin{bmatrix}1\\ e^{-2\lambda h_N}\end{bmatrix}}{[1,-1]\prod_{i=1}^{N-1}\mathbf{M}_i\begin{bmatrix}1\\ e^{-2\lambda h_N}\end{bmatrix}} \qquad [22]$$

Also, θ_i and ψ_i for the intermediate layer are

$$\theta_i(\lambda) = \frac{[1,0]\prod_{k=i}^{N-1}\mathbf{M}_k(\lambda)\begin{bmatrix}1\\ e^{-2\lambda h_N}\end{bmatrix}}{[1,-1]\prod_{k=1}^{N-1}\mathbf{M}_k(\lambda)\begin{bmatrix}1\\ e^{-2\lambda h_N}\end{bmatrix}}$$

$$\psi_i(\lambda) = \frac{[0,1]\prod_{k=i}^{N-1}\mathbf{M}_k(\lambda)\begin{bmatrix}1\\ e^{-2\lambda h_N}\end{bmatrix}}{[1,-1]\prod_{k=1}^{N-1}\mathbf{M}_k(\lambda)\begin{bmatrix}1\\ e^{-2\lambda h_N}\end{bmatrix}} \qquad [23]$$

Finally, the $2N$ $\theta_i(\lambda)$ and $\psi_i(\lambda)$ are found via solution of Eq. 23.

Using superposition, the voltage functions between the inner two probes for an N-layered specimen, for an inline four-point probe shown in Fig. 1, can be expressed as

$$\Delta V_i(S_2,z) = V_i(S_1,z) - V_i(S_1+S_2,z) + V_i(S_3,z) - V_i(S_2+S_3,z) \qquad [24]$$

Because the probes are in contact with specimen at the surface of the first layer ($z = 0$), the voltage function of the first layer by combining Eq. 22 and 24 is what we need to extract the electronic properties of each layer, from

$$V|_{z=0} = [V_1(S_1,0) - V_1(S_1+S_2,0) + V_1(S_3,0) - V_1(S_2+S_3,0)]$$

$$= \frac{I\rho_1}{\pi a}\int_0^\infty \frac{[1,1]\prod_{i=1}^{N-1}\mathbf{M}_i\begin{bmatrix}1\\ e^{-2\lambda h_N}\end{bmatrix}}{\lambda\left\{[1,-1]\prod_{i=1}^{N-1}\mathbf{M}_i\begin{bmatrix}1\\ e^{-2\lambda h_N}\end{bmatrix}\right\}}\{J_0(\lambda S_1) - J_0[2\lambda(S_1+S_2)] + J_0(\lambda S_3) - J_0[2\lambda(S_2+S_3)]\}\sin(\lambda a)d\lambda \qquad [25]$$

where $\mathbf{M}_i$ is defined in Eq. 19.

Numerical solutions for resistivities and contact resistances from experimental currents and voltages in the four-probe experiment.—As shown by Eq. 25, there are $2N-1$ unknowns (N electronic resistivities and $N-1$ contact resistances at each interface for an N-layered specimen as seen in Fig. 2, if no electrical properties within an N-layered specimen are known) with experimentally measured input current, I, probe radius, a, thickness of each layer, h_i, measured voltage, V, and probe spacing, S_i. Thus, $2N-1$ equations are required to determine $2N-1$ unknowns. The strategy adopted here is to change the probe spacing $2N-1$ times to obtain $2N-1$ different measured voltages, and then solve Eq. 25 numerically with the corresponding probe spacing sets and measured voltages, as illustrated in Fig. 4.

Solution for n parameters using n independent, nonlinear equations can generally be solved via Newton's method.[26] Briefly, variables x_i ($i = 1,2,\ldots,n$) are expressed as a tensor $\mathbf{F}(\mathbf{x})$, as

$$\mathbf{F}(\mathbf{x}) = \begin{bmatrix}F_1(\mathbf{x})\\ F_2(\mathbf{x})\\ \vdots\\ F_n(\mathbf{x})\end{bmatrix} = 0 \quad \text{where } \mathbf{x} = [x_1, x_2\ \cdots\ x_n] \qquad [26]$$

In the case of multilayered electrode, $\mathbf{F}_i$ is defined as

$$F_i(\mathbf{x}) = V_i|_{z=0} - V_i^{\text{measured}}$$

$$= \frac{I\rho_1}{\pi a}\int_0^\infty \frac{[1,1]\prod_{k=1}^{N-1}\mathbf{M}_k\begin{bmatrix}1\\ e^{-2\lambda h_N}\end{bmatrix}}{\lambda\left\{[1,-1]\prod_{k=1}^{N-1}\mathbf{M}_k\begin{bmatrix}1\\ e^{-2\lambda h_N}\end{bmatrix}\right\}} \times\begin{bmatrix}J_0(\lambda S_{(1,i)}) - J_0[2\lambda(S_{(1,i)}+S_{(2,i)})]\\ +\,J_0(\lambda S_{(3,i)}) - J_0[2\lambda(S_{(2,i)}+S_{(3,i)})]\end{bmatrix}\sin(\lambda a)d\lambda - V_i^{\text{measured}} \qquad [27]$$

where

$$\mathbf{M}_k(\mathbf{x}) = \begin{bmatrix}\dfrac{(x_{2k-1}+\lambda x_{2k}+x_{2k+1})}{2x_{2k+1}}, & -\dfrac{e^{2\lambda h_k}(x_{2k-1}+\lambda x_{2k}-x_{2k+1})}{2x_{2k+1}}\\ \dfrac{e^{-2\lambda h_k}(-x_{2k-1}+\lambda x_{2k}+x_{2k+1})}{2x_{2k+1}}, & \dfrac{(x_{2k-1}-\lambda x_{2k}+x_{2k+1})}{2x_{2k+1}}\end{bmatrix}$$

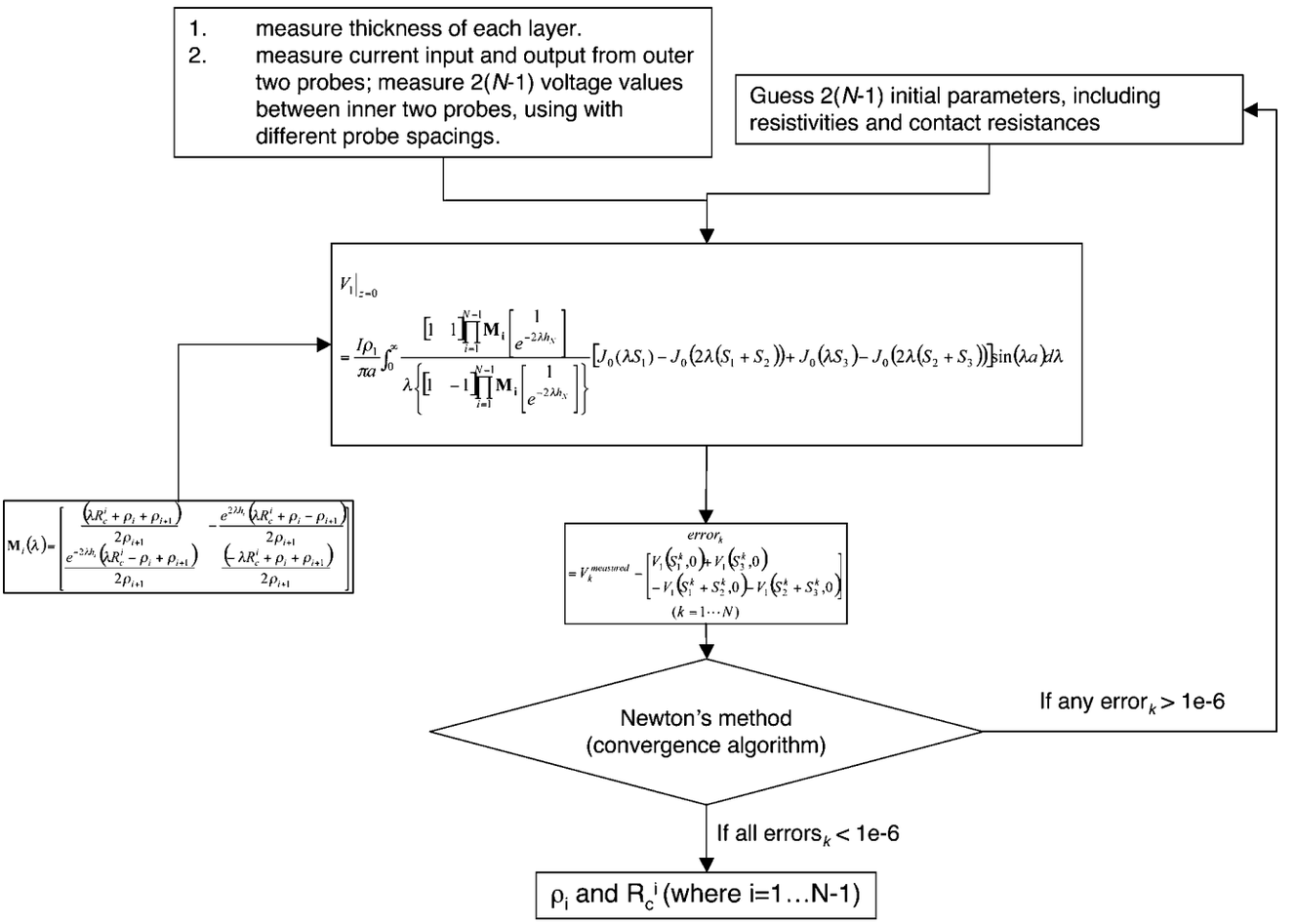

Figure 4. Flow chart of experimental approach and data reduction.

and $S_{(j,i)}$ stands for the jth probe spacing at the ith set, j is ranged from 1 to 3, but i is ranged from 1 to n depending on how many unknowns

$$\mathbf{x} = [x_1, x_2, \ldots, x_n] \qquad [28]$$

The odd terms in tensor $\mathbf{x}$ are resistivities, and the even terms are contact resistances. Unknown variables x_is comprise N electronic resistivities and $N - 1$ contact resistances in an N-layered specimen. The algorithm of prediction of error of the $(j + 1)$-th step can be expressed in terms of the error of the jth step, $\nabla^2\mathbf{F}$ and inverse of Jacobean $\mathbf{J}(\mathbf{x}^j)$ tensor as

$$\mathbf{e}^{j+1} = (\mathbf{x}^{j+1} - \mathbf{r}) = -\mathbf{J}(\mathbf{x}^j)^{-1}\nabla^2\mathbf{F}(\mathbf{x}^{j-1})(\mathbf{e}^j)^{2'} \qquad [29]$$

The $\mathbf{r}$ comprises the roots of $\mathbf{F}(\mathbf{x})$. Also, the $(j + 1)$-th step of x^{j+1} can be determined by expanding $\mathbf{F}(\mathbf{x})$ in terms of Taylor series and neglecting higher order terms as

$$\delta\mathbf{x}^i = -\mathbf{J}(\mathbf{x}^j)^{-1}\mathbf{F}(\mathbf{x}^j) \qquad [30]$$

$$\mathbf{x}^{j+1} = \mathbf{x}^j + \delta\mathbf{x}^j$$

The roots of $\mathbf{F}(\mathbf{x})$ can be obtained by calculation of Eq. 29 iteratively until convergence is obtained.

The central advantage of Newton's method is its quadratic convergence, for sufficiently accurate initial seeds, as illustrated in Eq. 29. This approach has two major disadvantages, which we address presently, for the application at hand. First, function evaluation as in Eq. 30 can be time-consuming, because a system of n equations requires $n^2 + n$ function evaluations for each step; this includes n^2 elements of Jacobian matrix, $\mathbf{J}(\mathbf{x}^i)$, and n elements of $\mathbf{F}(\mathbf{x}^j)$ determined from Eq. 25. Further, it is frequently difficult to obtain the Jacobian analytically as shown by Eq. 30; in such cases, computational intensiveness is even greater, because the Jacobian must be found numerically, *e.g.*, via forward finite difference estimation, with suitably small trial forward steps. Here, we carried out both analytical and numerical estimations of the Jacobian tensor, finding the differences in our results to be small. Results reported here are thus based on the analytical approximation of Eq. 30.

The second major disadvantage of Newton's method is its tendency to diverge for insufficiently accurate seeds. Specifically, if the iterative procedure of Eq. 30 approaches a horizontal asymptote or a local extreme, the prediction offset, $\delta\mathbf{x}^i$ of Eq. 30 could produce wandering. As seen in Eq. 29, the error, $\mathbf{e}^{j+1}$, converges quadratically if seeds are close to roots; it diverges quadratically if seeds are far from the roots. Following a commonly used method to guarantee global convergence,[26,27] $\delta\mathbf{x}^j$ was factorized by a factor s as in Eq. 31. The factor s is determined to assure the increment minimizing $f(\mathbf{x}^j) = |\frac{1}{2}\mathbf{F}(\mathbf{x}^j) \cdot \mathbf{F}(\mathbf{x}^j)|$, other than of increase full step to assure convergences as

$$\delta\mathbf{x}^i = -\mathbf{J}(\mathbf{x}^j)^{-1}\mathbf{F}(\mathbf{x}^j) \qquad [31]$$

$$\mathbf{x}^{j+1} = \mathbf{x}^j + s\delta\mathbf{x}^j$$

where $0 < s \leqslant 1$.

The approach adopted here[26] is described as follows. During each iteration, the full Newton step is taken at first, as in Eq. 29. However, we check on f with the full increment. If the prediction increment δx^j, leads to an increase in f, we backtrack with factor s as in Eq. 31 until we have an acceptable step; this method is guaranteed to find an acceptable step. The criterion to find s in Eq. 31 thus assures that f decreases, and satisfies

$$f(\mathbf{x}^{j+1}) \leqslant f(\mathbf{x}^j) + 10^{-4} \cdot \nabla f \cdot (\mathbf{x}^{j+1} - \mathbf{x}^j) \quad [32]$$

The reason we use Eq. 32 instead of $f(\mathbf{x}^{j+1}) < f(\mathbf{x}^j)$ is that a sequence of steps might satisfy $f(\mathbf{x}^{j+1}) < f(\mathbf{x}^j)$, but reduces f too slowly, relative to step lengths. If the full Newton step fails to satisfy the criterion in Eq. 32, then s is determined from

$$s = -\frac{\nabla f(\mathbf{x}^j) \cdot \delta \mathbf{x}^j}{2[f(\mathbf{x}^{j+1}) - f(\mathbf{x}^j) - \nabla f(\mathbf{x}^j) \cdot \delta \mathbf{x}^j]} \quad [33]$$

If the value of s determined from Eq. 33 still does not satisfy Eq. 32, the subsequent backtracking factor, s, is determined as follows. First, a new function, g, is defined as

$$g(s) = cs^3 + ds^2 + [\nabla f(\mathbf{x}^j) \cdot \delta \mathbf{x}^j]s + f(\mathbf{x}^j) \quad [34]$$

where c and d are determined by

$$\begin{bmatrix} c \\ d \end{bmatrix} = \frac{1}{s_1 - s_2} \begin{bmatrix} \frac{1}{s_1^2} & -\frac{1}{s_2^2} \\ -\frac{s_2}{s_1^2} & \frac{s_1}{s_2^2} \end{bmatrix} \cdot \begin{bmatrix} g(s_1) - g(0) - s_1 g'(0) \\ g(s_2) - g(0) - s_2 g'(0) \end{bmatrix} \quad [35]$$

The s_1 and s_2 are the previous and second-most recent values of s, respectively. The new s to assure a minimum of Eq. 34 is found from

$$s = \frac{-d + \sqrt{d^2 - 3cg'(0)}}{3c} \quad [36]$$

and is selected in the range $s_{max} = 0.5s_1$ and $s_{min} = 0.1s_1$.

As stated earlier, $2 \cdot N - (M + 1)$ measurements are required for solution, obtained by using different sets of probe spacing and measured voltages, where N is the number of layers and M is the number of layers of known electronic conductivities. The experimental technique for obtaining these data follows.

Experimental approach.—The four-layered laminated $LiFePO_4$ cathodes consisted of active material: a carbon-coated $LiFePO_4$ (PhosTech, Canada), acetylene black (AB) and/or graphite (G) bonded with poly(vinyl difluoride) (PVdF), and cast onto a three-layered carbon-coated Al current collector as in Fig. 5. The $LiFePO_4$ powder was coated with 1-2 wt % carbon during synthesis. $LiFePO_4$ cathodes were prepared at Hydro-Québec (HQ-IREQ). Compositions are listed in Table I; all cathodes were pressed after air-drying, and all measurements reflect post-pressing dimensions. Volume fraction (vf %) of each constituent listed in Table I was calculated based on mass of densities of $LiFePO_4$ (3.6 g/cm[312]), PVdF (1.76 g/cm[311]), carbon and graphite (2.25 g/cm[311]).

The inline four-point-probe setup of Fig. 1 was used on these cathodes as illustrated by Fig. 5. During testing, each specimen was placed on a flat, insulating, Plexiglass stage, as shown. A small input current was delivered through one outer probe and withdrawn from an inner probe. A Digatron charge/discharge unit was used to deliver and withdraw current, and an HP-34401A multimeter was used to measure voltage drops between the second and third (inner) two probes.

Generally, the number of different sets of probe spacing required is $2N - (M + 1)$, where N is the number of the layer within the multilayered electrode, and M is the number of layers of known electronic resistivity. In our four-layered structure, four independent sets of probe spacing (S_1,S_2,S_3) were used to determine electronic

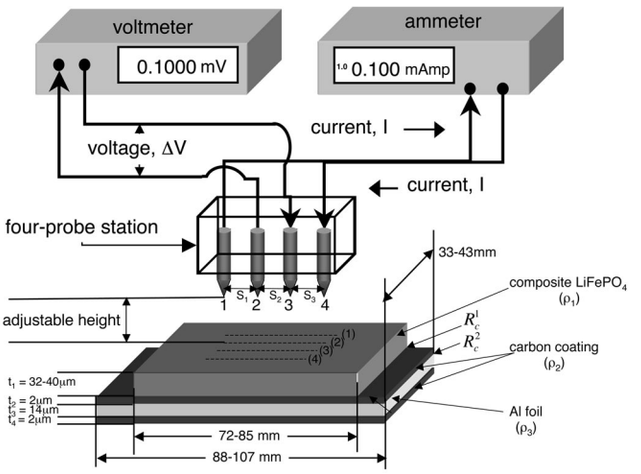

Figure 5. Schematic test apparatus used in the measurement of electronic conductivities and contact resistances and approximate dimension of specimen. The dotted lines (1)-(4) represent possible locations of probes for various probe settings.

conductivities (ρ_1 and ρ_2) and contact resistances (R_c^1 and R_c^2 at interfaces of (1, 2) and (2, 3) layers, as shown in Fig. 5. This is a reduction of the $2N - (M + 1) = 2^*3 - (1 + 1) = 4$ equations theoretically required; (t_1,t_2,t_3), ρ_3, and different sets of (S_1,S_2,S_3) values were thus assumed.

These assumptions included the resistivity of the Al foil current collectors, of $\rho_3 = 3.0\ \mu\Omega$ cm,[11] and a negligible conductivity of the fourth layer, *i.e.*, ρ_4 = infinity. The latter assumption was made because of the negligible current flow in the fourth layer, which in turn results from the much lower conductivity in the carbon layer (layer 4) than the Al foil layer (layer 3). Together, these assumptions effectively reduced the four-layered structure into a three-layered structure, for purposes of analysis.

Limitations of measurement locations relative to sample size were previously suggested by Schroder[28] to assure precision in four-probe experiments. These limitations were followed here: distances from the edge probes (probe 1 or 4) to the nonconducting edge, and distances from the each probe center to a nonconducting edge were kept at least three times larger than the largest probe spacing from the specimen edge.

Our measurements at each location were taken for four different probe settings (2.8,2.8,2.8 mm), (5.6,2.8,2.8 mm), (2.8,5.6,2.8 mm), and (2.8,5.6,5.6 mm), on the cathode surface. Thus, a total of four different voltages were measured at each location with four different probe settings (S_1,S_2,S_3) as described previously. Four sets of data, at four different locations (1), (2), (3), and (4) as indicated in Fig. 5 [of four different spacing settings (S_1,S_2,S_3) each] were taken at each electrode. Hence, total of 16 voltages were measured; four for each location.

The measured voltages taken at each location were averaged and analyzed according to the technique outlined previously, to extract electronic properties. The same procedure was repeated for the remaining three sets of voltages, to obtain variability in electronic conductivity and contact resistance. A flow chart of the procedure used is shown in Fig. 4.

Results

Table II summarizes our findings on resistivities and contact resistances for the five electrodes studied. We divide our comments into three parts: (*i*) effect of carbon and (*ii*) graphite additives, respectively, on resistivities and contact resistances, and (*iii*) effects of

Table I. List of constituents of composite $LiFePO_4$ cathode materials.

Electrode number	$LiFePO_4$ (wt %)	$LiFePO_4$ (vf %)	PVdF (wt %)	PVdF (vf %)	Carbon black (wt %)	Carbon black (vf %)	Graphite (wt %)	Graphite (vf %)	Length (mm)	Composite $LiFePO_4$ length (mm)	Width (mm)	Total thickness (μm)	Composite $LiFePO_4$ thickness (μm)	Carbon coating thickness (μm)	Al foil thickness (μm)	Density (g/cm^3)
1	85	26	12	7	3	1.4	–	–	100.8	76.68	46.73	52	34	2	14	1.71
2	82	24	12	7	6	2.8	–	–	96	72.16	44.54	52	34	2	14	1.49
3	78	17	12	5	10	3.6	–	–	95.8	71.98	33.33	50	32	2	14	1.28
4	79	24	12	7	3	1.5	6	3.0	106.5	75.85	41.21	58	40	2	14	1.52
5	76	22	12	7	6	2.8	6	2.8	90	72.4	43.25	51	33	2	14	1.41

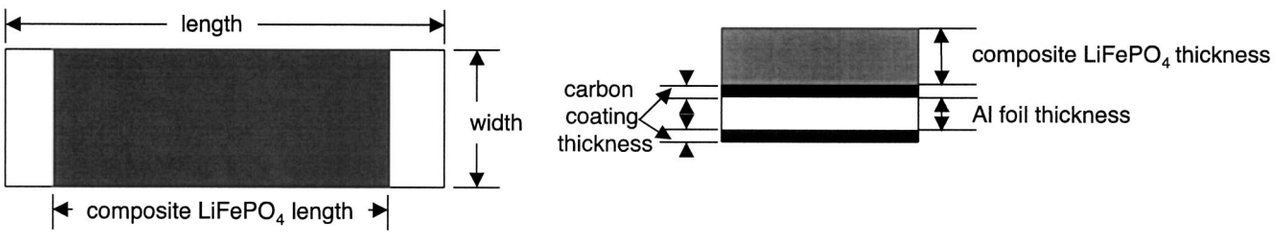

carbon coatings on interfacial resistances. Results are reported in Fig. 6.

Effect of amount of carbon additives on resistivities/contact resistance.—Figure 6a reports resistivities of $LiFePO_4$ matrix for all electrodes studied. For electrodes 1-3 which only have carbon black additive, the average of electronic resistivity decreased from 176 to 46 Ω cm as the carbon content increased from 3 to 6 wt % (1.4-2.8 vf %), but increased from 46 to 67 Ω cm as the carbon content increased from 6 to 10 wt % (2.8-3.6 vf %). The variation of electronic resistivity decreased within electrode as the carbon contents increased. Similarly, for electrodes 4 and 5 that have both carbon black and graphite additives, the electronic resistivies decreased from 353 to 59 Ω cm as the carbon black content increased from 3 to 6 wt % (1.5 to 2.8 vf %).

Figure 6b shows that contact resistance at the interface (the first interface) of $LiFePO_4$ matrix and carbon coating of current collector layers of electrodes 1-3, which have carbon black conductive additives only, decreased from 1.62 to 0.77 Ω cm^2 and then increased to 1.84 Ω cm^2 as the carbon contents increased from 3 to 10 wt % (1.4-3.6 vf %). The standard deviation of contact resistance at the first interface decreased from 1.09 to 0.77 Ω cm^2 and slightly increased to 0.72 Ω cm^2 as the carbon black content increased. However, the contact resistance at the first interface of electrodes 4 and 5, which have both carbon black and graphite additives, increased from 0.85 to 1.21 Ω cm^2 as carbon black content increased from 3 to 6 wt % (1.5-2.8 vf %).

Effect of graphite additives on resistivity/contact resistance.—Figure 6a shows that resistivities of $LiFePO_4$ matrix of electrodes 1 and 4 increased from 176 to 353 Ω cm as the graphite content increased from 0 to 6 wt % (0-3 vf %). But resistivities of electrodes 2 and 5 decreased from 67 to 59 Ω cm as the graphite contents increased from 0 to 6 wt % (0-2.8 vf %). The standard deviation of electronic resistivity of $LiFePO_4$ matrix of electrodes 1 and 4 increased from 122 to 238 Ω cm, while the standard deviation of electronic resistivity of electrodes 2 and 5 decreased 32-10 Ω cm.

Figure 6b showed that contact resistance at the interface (the first interface) of composite $LiFePO_4$ active material and carbon coating of current collector layers of electrodes 1 and 4, which have 3 wt % carbon black conductive additives, decreased from 1.62 to 0.85 Ω cm^2 as the graphite contents increased from 0 to 6 wt % (0-3 vf %). But the contact resistance of the first interface of electrodes 2 and 5, which both have 6 wt % of carbon black additives, increased from 0.77 to 1.21 Ω cm^2 as the graphite additive contents increased from 0 to 6 wt % (0-2.8 vf %). The standard deviation of contact resistance at the first interface of electrodes 1 and 4 decreased from 1.09 to 0.72 Ω cm^2 as the graphite contents

Table II. Measured electronic resistivities and resistances for each layer of the multilayered $LiFePO_4$ cathodes studied.

	Composite $LiFePO_4$ (Ω cm)		Contact resistance at 1st interface (Ω cm^2)		Carbon layer (Ω cm)		Contact resistance at 2nd interface (Ω cm^2)	
	Mean	Standard deviation	Mean	Standard deviation	Mean	Standard deviation	Mean	Standard deviation
1	1.76×10^2	1.22×10^2	1.62×10	1.09	9.47×10^{-3}	2.48×10^{-3}	2.44	2.57×10^{-1}
2	4.57×10^1	3.29×10^1	7.68×10^{-1}	2.34×10^{-1}	1.14×10^{-2}	7.38×10^{-3}	1.50	1.68×10^{-1}
3	6.69×10^1	3.91×10^1	1.84	7.24×10^{-1}	9.72×10^{-3}	6.24×10^{-3}	3.08	1.57
4	3.53×10^2	2.38×10^2	8.45×10^{-1}	7.06×10^{-1}	4.14×10^{-2}	3.11×10^{-2}	3.33	6.53×10^{-1}
5	5.90×10^1	1.00×10^1	1.21	6.23×10^{-1}	8.96×10^{-3}	3.95×10^{-3}	2.56	1.91×10^{-1}

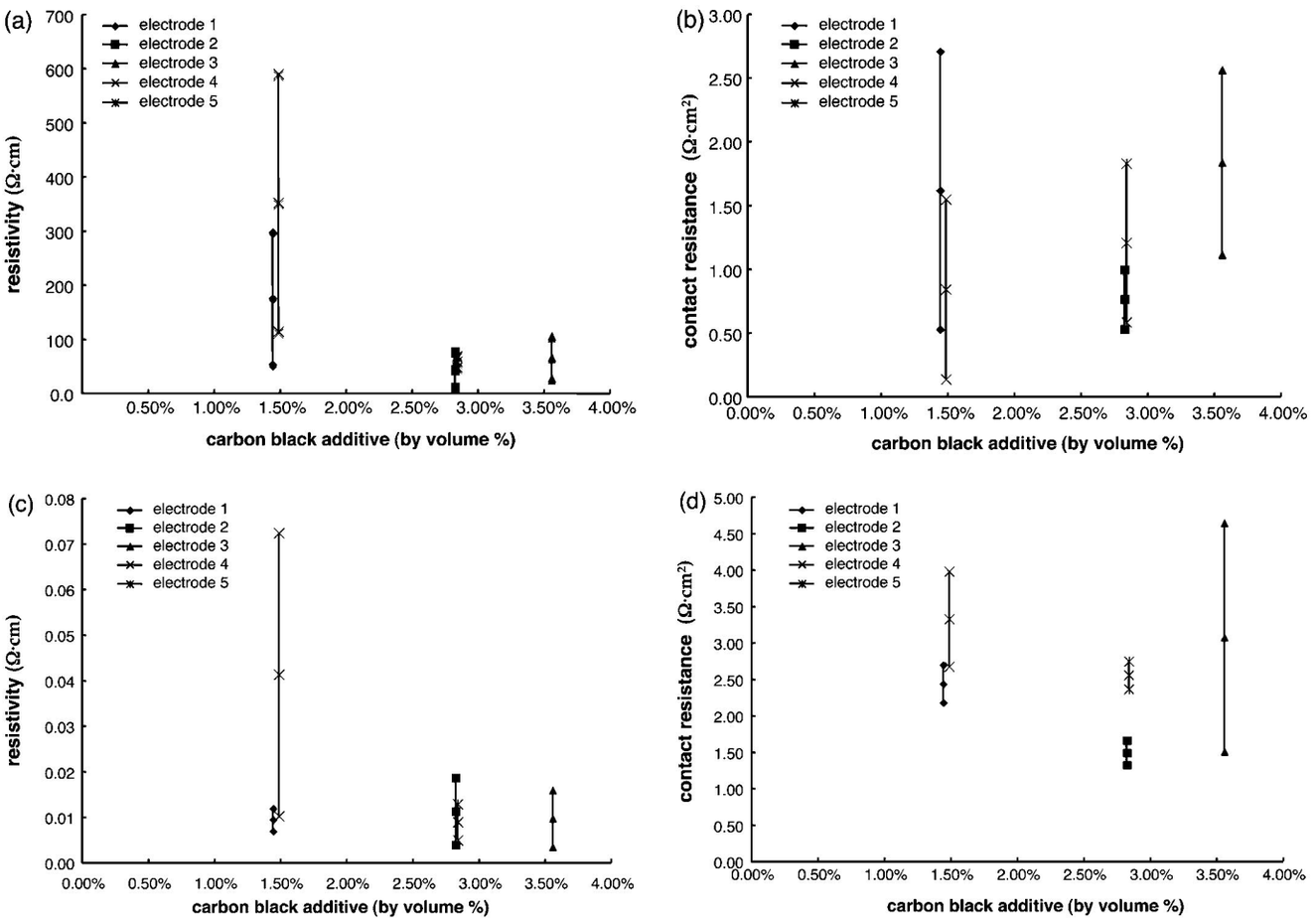

Figure 6. Bar charts of mean and standard deviations ($\pm 1\sigma$) of (a) electrical resistivity of composite $LiFePO_4$ active materials, (b) contact resistances at interfaces of composite $LiFePO_4$ and the carbon coatings on Al current collectors, (c) electronic resistivities of carbon coatings on current collectors, and (d) contact resistances at interfaces of carbon coating and Al foil current collectors.

increased. However, the contact resistance at the first interface of electrodes 2 and 5 increased from 0.23 to 0.62 Ω cm^2 as the graphite additive contents increased from 0 to 6 wt % (0-2.8 vf %).

Effects of additives on interlayer properties.—Figure 6c shows that the top layers of double-sided carbon-coated current collector (Al foil) had approximately equal values for all electrodes ($\sim$10,000 $\mu\Omega$ cm), except electrode 4 (41,400 $\mu\Omega$ cm).

Figure 6d shows that the contact resistance of interface (the second interface) between the top layer of double-sided carbon-coated of current collector and metal current collector (Al foil) was $\sim$2.6 Ω cm^2 for all electrodes.

Discussion

Effect of amount of carbon black additives on resistivities.—The decrease in standard deviation of electronic resistivity of $LiFePO_4$ matrix of electrodes 1-3, from 122 to 39 Ω cm, with increasing carbon black content is indicative of homogeneity in packing of percolated carbon black particles. Given the difficulty in estimation of volume fractions and final particle shapes in these pressed structures, this is useful information in verifying that particle fractions are significantly above those required for percolation.

Effect of amount of graphite additives on resistivities.—The effects of graphite conductive additives cannot be satisfactorily assessed from our results (Table II and Fig. 6a), because the resistivity of composite $LiFePO_4$ active material of electrode 4 significantly deviated from that of the other electrodes. This electrode exhibited both high mean and standard deviation (353 and 238 Ω cm) compared to values for the other electrodes studied (46-173 Ω cm, and 10-122 Ω cm, respectively). Carbon black contents were identical for electrodes 1 and 4 (1.5 vf %) and 2 and 5 (2.8 vf %). Comparison of conductivity for these electrodes thus showed that carbon black additives had little effect on conductivity, but graphite additives had a clear effect. Electrode 4, with 3 vf %, and electrode 5, with 2.8 vf % graphite, each were of much higher resistivity than the other electrodes. Thus, addition of graphite actually appeared to reduce overall conductivity in the materials studied. Also, the increasing amount of graphite content (volume fraction aspect) has less effect on improving $LiFePO_4$ matrix conductivity, as shown in Fig. 6a.

Per Table I, electrodes 3-5 had similar weight percentages of $LiFePO_4$ and PvdF; both constituents comprised about 90 wt % of the composite $LiFePO_4$ matrix in these electrodes. Their resistivities were also similar ($\sim$63 Ω cm), except electrode 4 that has resistivity of 353 Ω cm. We expected electrode 4 to exhibit lower resistivity than electrode 1, because it contained a smaller fraction of insulating $LiFePO_4$ particles and the same fractions of PVdF and carbon black, but instead, this electrode exhibited the highest value among all electrodes: its resistivities exceeded those of other electrodes (electrodes 3 and 5) by a factor of 4. Also, the contact resistance of the first interface of electrode 4 had a low mean value and

large standard deviation, but the contact resistance of the second interface of electrode 4 had the highest average value measured among electrodes 3 to 5. Furthermore, the resistivity of carbon coating at the second layer for electrode 4 has the highest value among all electrodes.

One possible reason for these results is that for electrode 4, pressing during manufacturing lead to electrode fracture and attendant high resistivity of the composite $LiFePO_4$ matrix. As shown previously,[18] excessive compression of electrodes can result in particle breakage within them, which cancels out the potential benefit of increasing contact among particles and current collectors. Here the compressed active material matrix of electrode 4 may have become excessively intermingled with the carbon coating of the current collector, resulting in the low observed contact resistance at the first interface but high resistivity of the carbon layer.

For electrodes 2 and 5, average resistivities of $LiFePO_4$ matrix increased slightly from 46 to 59 Ω cm, but the standard deviation decreased from 33 to 10 Ω cm, as the graphite particle content increased from 0 to 10 wt %. It thus seems that graphite does not improve the electronic conductivity as effectively as carbon black but can produce homogeneous layers. This may be due to the different morphologies of graphite particles and carbon black particles, as discussed previously in Ref. 18.

More generally, the standard deviation of resistivities measured in the $LiFePO_4$ matrix layers decreased as conductive additive content increased above 6 wt %, as demonstrated by data from electrodes 2, 3, and 5. This may again be an indication that the percolation threshold for conductive additive is higher than 6 wt % for both carbon black and graphite.

Effects of additives on interlayer properties.—The nearly uniform resistivities of carbon layers in all electrodes ($\sim$10000 Ω cm), except electrode 4, verifies the uniformity of carbon produced for, and deposited within, these layers.

Because contact resistance is inversely proportional to contact area, it serves as an indication of state of contact between particles and current collector. Generally, the contact resistances at interfaces between the $LiFePO_4$ composite layers and the upper carbon coating of current collector (first interface) were within the same range, of $\sim$1.25 Ω cm^2. Similarly, contact resistances at the interface of the upper carbon coating layer and Al metal current collector (second interface) of the electrodes studied, were within the same range, of $\sim$2.58 Ω cm^2. The slightly higher contact resistances of electrode 3 for the first and second interfaces indicate possible compression-induced failures of particles; this hypothesis is consistent with the slightly increased resistivity of $LiFePO_4$ matrix observed in this case, even though the carbon content was higher. Similarly high contact resistance of the second interface of electrode 4 could be due to fracture of the particles. Otherwise, results were fairly consistent.

Selection of particle sizes.—Particle size directly affects electrochemical performance; larger particle sizes of $LiFePO_4$, for example, result in longer ion diffusion times in cathodes. Thus, smaller particles with high specific surface area have potentially higher achievable capacity. Goodenough and Manivannan[29] have suggested the optimal cathode performance is achievable with uniformly small sizes of $LiFePO_4$ particles; this has also been substantiated by Yamada and co-workers[30] and Takahashi *et al.*[31] for carbon-coated $LiFePO_4$ particles. However, smaller particles have larger surface areas, and thus more carbon additive is required to improve conductivity, which sacrifices energy density. Indeed, Chen and Dahn[12] have pointed out that increases of carbon additive, from 0 to 15 wt %, reduce volumetric energy density by 22% and gravimetric energy density by 15%.

Modification of surface chemistry of $LiFePO_4$ particles requires heating, which in turn alters the conductivity of carbon additives.[32] Kostecki and co-workers[33] recently used current-sensing atomic force microscopy (AFM) images to quantify local alterations in electronic conductivity of carbons. Collectively, these results suggest that surface treatments of particles, particle size distributions, and analysis and measurements of conductivity must be made in concert to improve $LiFePO_4$ systems. Additionally, the risk of fracture of larger particles under the compression is generally greater, and work here suggests that dramatic increases in both layer-wise resistivities and contact resistances may result from such structural failures.

Numerical issues.—The modified Newton's method used here to solve the nonlinear equations of Eq. 25, with increment reduction as per Eq. 31, required good initial guesses for each parameter sought. This proved to be a time-consuming step in reducing experimental data.

Electronic resistivities of each layer in the multilayered electrode were required to be in decreasing order starting from the electrode surface where the four-point probes were placed (*i.e.*, the resistivity of a layer needed to be equal to or larger than that for the layer below it). If the electronic resistivity of a layer were much larger than the one above it, calculated contact resistance at the interface between the two layers was high, indicating that no current reached the next layer. Thus, if the electronic resistivities of multilayered electrode were not in decreasing order, the number of layers needed to be reduced. For example, the electrodes studied here had four layers (composite $LiFePO_4$ matrix, first carbon coating, Al metal current collector, and second carbon coating as shown in Fig. 5). But the resistivity of the second carbon coating at the fourth layer was much larger than the Al metal current collector at the third layer. The number of layers was thus reduced to three, as discussed previously.

Conclusions

Extension of the Schumann-Gardner approach to measure the electronic properties of multilayered electrodes was successfully made, and data from an inline four-point-probe technique were used to determine resistivities of $LiFePO_4$ matrix and carbon coatings on current collectors, and contact resistances at each interface in the cathodes studied. Overall, we found that carbon black additives improved electronic resistivity of $LiFePO_4$ to greater extent than graphite additives.

Based on results here, we suggest that addition of $\sim$3 vf % carbon black significantly improves electronic conductivity of $LiFePO_4$ composite cathodes. Addition of graphite additives was shown to be of less benefit in improving electronic conductivity of these cathodes. Consistent resistivities of contact resistances at interfaces with carbon coatings among the electrodes studied suggests that the manufacturing approach used to make them is consistent.

Our general approach may ultimately prove useful in determining the optimal thicknesses of conductive coating around $LiFePO_4$ particles, or optimal fractions of conductive additives for improved electronic conductivity of $LiFePO_4$ matrix, with acceptable volumetric and gravimetric energy density. One possible element of future work may be to combine the experimental technique developed with mathematical models for the thin electrodes[14,18] to simultaneously identify percolation thresholds for different morphologies of conductive additives, and also predict the effect of particle morphology and type on capacity. Verification of electrochemical performance of these cells will also be part of future work.

Acknowledgments

This work was generously supported by the U.S. Department of Energy BATT Program (Dr. Tien Duong, Program Director, DOE). Additional support was provided by an NSF PECASE Award (Sastry). We gratefully acknowledge these sponsors and colleagues.

The University of Michigan assisted in meeting the publication costs of this article

List of Symbols

A	probe radius
A_i	a function of λ used in solving the *i*th layer voltage function
B_i	a function of λ used in solving the *i*th layer voltage function
$\mathbf{F}$	a tensor used in Newton's method
F_i	the *i*th element of **F** tensor
h_i	distance from electrode surface to the bottom of the *i*th layer
I	current
$\mathbf{J}$	Jacobean tensor
J_0	a Bessel functions of the first kind
M	number of layers with known electronic resistivities
$\mathbf{M}_i$	a matrix function
N	number of layers for multilayered electrode
P	power
Q	power of heat source
r	radius direction in cylindrical coordinate
R_f	reflectivity at the surface of the first layer
R_i	a function of r only appears in solving Laplace equation with separation of variables approaches
R_c^i	contact resistance at the *i*th interface (between the *i*th and the (*i* + *1*)th layers)
s	backtracking factor
S_i	*i*th probe spacing
V_i	*i*th layer voltage
$V_i^{measured}$	experimentally measured voltage via the *i*th probe spacing set
$\mathbf{x}$	a tensor of independent variables
x_i	the *i*th element of **x** tensor
z	depth direction in cylindrical coordinate
Z_i	a function of z only appears in solving Laplace equation with separation of variables approaches

Greek

α_1	optical absorption coefficient
λ	a constant appears in solving Laplace equation
θ_i	a function of λ used in solving the *i*th layer voltage function
ρ_i	resistivity of the *i*th layer within multilayered electrode
ω	angular frequency
ψ_i	a function of λ used in solving the *i*th layer voltage function

References

1. S. Y. Chung, J. T. Bloking, and Y. M. Chiang, *Nat. Mater.*, **1**, 123 (2002).
2. A. K. Padhi, K. S. Nanjundaswamy, C. Masquelier, S. Okada, and J. B. Goodenough, *J. Electrochem. Soc.*, **144**, 1609 (1997).
3. H. Huang, S. C. Yin, and L. F. Nazar, *Electrochem. Solid-State Lett.*, **4**, A170 (2001).
4. N. Ravet, Y. Chouinard, J. F. Magnan, S. Besner, M. Gauthier, and M. Armand, *J. Power Sources*, **97**, 503 (2001).
5. J. Shi, A. A. Massucco, and D. G. Fauteux, U.S. Pat. 5,580,686 (1996).
6. M. Gauthier, S. Besner, M. Armand, J.-F. Magnan, H. Hamelin, and A. Belanger, U.S. Pat. 6,485,866 (2002).
7. C. W. Wang, K. A. Cook, and A. M. Sastry, *J. Electrochem. Soc.*, **150**, A385 (2003).
8. F. Croce, A. D. Epifanio, J. Hassoun, A. Deptula, T. Olczac, and B. Scrosati, *Electrochem. Solid-State Lett.*, **5**, A47 (2002).
9. R. Dominko, M. Gaberscek, J. Drofenik, M. Bele, and J. Jamnik, *Electrochim. Acta*, **48**, 3709 (2003).
10. S. L. Bewlay, K. Konstantinov, G. X. Wang, S. X. Dou, and H. K. Liu, *Mater. Lett.*, **58**, 1788 (2004).
11. http://www.matweb.com
12. Z. H. Chen and J. R. Dahn, *J. Electrochem. Soc.*, **149**, A1184 (2002).
13. Y. B. Yi and A. M. Sastry, *Phys. Rev. E*, **66**, 066130 (2002).
14. Y. B. Yi and A. M. Sastry, *Proc. R. Soc. London, Ser. A*, **460**, 2048, 2353 (2004).
15. M. F. Sykes and J. W. Essam, *Phys. Rev. Lett.*, **10**, 1,3 (1963).
16. A. Drory, *Phys. Rev. E*, **55**, 3878 (1997).
17. R. Dominko, M. Gaberscek, J. Drofenik, M. Bele, S. Pejovnik, and J. Jamnik, *J. Power Sources*, **119**, 770 (2003).
18. C. W. Wang, Y. B. Yi, A. M. Sastry, J. Shim, and K. A. Striebel, *J. Electrochem. Soc.*, **151**, 9,A1489 (2004).
19. P. A. Schumann and E. E. Gardner, *Solid-State Electron.*, **12**, 371 (1969).
20. P. A. Schumann and E. E. Gardner, *J. Electrochem. Soc.*, **116**, 87 (1969).
21. M. S. Leong, S. C. Choo, and C. C. Wang, *Solid-State Electron.*, **20**, 255 (1977).
22. P. J. Severin, Semiconductor Measurement Technology: Spreading Resistance Symposium, in *Nbs Special Publication*, p. 27 (1974).
23. H. L. Berkowitz and R. A. Lux, *J. Electrochem. Soc.*, **126**, 1479 (1979).
24. S. C. Choo, M. S. Leong, and K. L. Kuan, *Solid-State Electron.*, **19**, 561 (1976).
25. B. C. Li and S. Y. Zhang, *J. Phys. D*, **30**, 1447 (1997).
26. W. H. Press, *Numerical Recipes in Fortran 77: The Art of Scientific Computing*, 2nd ed., Cambridge University Press, Cambridge, England (1996).
27. K. E. Atkinson, *An Introduction to Numerical Analysis*, 2nd ed., Wiley, New York (1989).
28. D. K. Schroder, *Semiconductor Material and Device Characterization*, 2nd ed., Wiley, New York (1998).
29. J. B. Goodenough and V. Manivannan, *Denki Kagaku oyobi Kogyo Butsuri Kagaku*, **66**, 1173 (1998).
30. A. Yamada, S. C. Chung, and K. Hinokuma, *J. Electrochem. Soc.*, **148**, A224 (2001).
31. M. Takahashi, S. Tobishima, K. Takei, and Y. Sakurai, *J. Power Sources*, **97-8**, 508 (2001).
32. P. Delhaes and F. Carmona, in *Chemistry and Physics of Carbon*, M. Dekker, New York (1965).
33. R. Kostecki, B. Schnyder, D. Alliata, X. Song, K. Kinoshita, and R. Kotz, *Thin Solid Films*, **396**, 36 (2001).